Surface layers overlap and effective adhesion in reverse micelles: A discussion from the adhesive spheres mixture model

S. Amokrane and C. Regnaut

Citation: J. Chem. Phys. **106**, 376 (1997); doi: 10.1063/1.473201
View online: http://dx.doi.org/10.1063/1.473201
View Table of Contents: http://jcp.aip.org/resource/1/JCPSA6/v106/i1
Published by the AIP Publishing LLC.

Surface layers overlap and effective adhesion in reverse micelles: A discussion from the adhesive spheres mixture model

S. Amokrane and C. Regnaut
Laboratoire de Physique des Milieux Désordonnés, Faculté des Sciences et de Technologie, Université de Paris 12 Val de Marne, 61 Avenue du Général de Gaulle, 94010 Créteil Cedex, France

(Received 6 August 1996; accepted 25 September 1996)

Structural data on reverse micelles from the literature are analyzed from the adhesive spheres mixture model in the Percus–Yevick approximation. The solvent is modeled by a fluid of pseudoadhesive spheres with same compressibility and coordination number as a square well fluid. The attractive part of the direct intermicellar potential is taken proportional to the overlap volume of interpenetrating surface layers. The micelle–solvent coupling is characterized by a square or triangular well and a constraint on the packing fractions. A very good correlation is then found between the micelles stickiness parameters computed from the actual potentials via the equality of second virial coefficients and those determined from a fit to experiment. The change in effective adhesion observed with micelles of different surface composition and in the same solvent can then be associated to the change in the direct intermicellar interaction at nearly unchanged solvent–micelle interactions. The interpretation of the role of the overlap volume resulting from this multicomponent approach is contrasted with that based on approximate calculations of the potential of mean force. © *1997 American Institute of Physics.* [S0021-9606(97)50701-X]

I. INTRODUCTION

As exemplified by the results of light scattering measurements, structural data on water in oil microemulsions indicate that the effective interaction of reverse micelles is strongly affected by the composition of their surface. Among others, the data of Brunetti *et al.*[1] on the influence of the cosurfactant chain length provide one of the most convincing evidence of this. A theoretical explanation of the experimental observation that the effective attraction is stronger the shorter the alcohol was proposed starting from an intermicellar potential of mean force including van der Waals attractions and repulsive contributions in overlapping surface layers.[2] Good agreement with the experimental osmotic second virial coefficient was found though the magnitude of the computed potential is rather sensitive to the precise value of the volume per CH_2 group at the interface. Nevertheless, this approach outlined a qualitatively important aspect, that is the crucial role of the overlap volume of interpenetrating surface layers. This conclusion was confirmed by the investigation of the role of the surfactant chain length.[3]

This theoretical model raises, however, the question of the specificity of the suspending medium. Indeed, the latter was actually not considered as made of truly discrete species. In particular, the van der Waals attraction was computed according to a Hamaker's scheme in which the surface layers overlap induces removing of continuous phase. The suspending medium is thus characterized only by the change in molar partial volume inside and outside the aliphatic layer. More recent work on various colloidal systems suggests, however, a different picture of the role of the solvent. For instance, depletion induced phase separation emphasizes the role of hard core exclusion effects.[4,5] Coated silica particles are also known to behave differently in cyclohexane[6] and in benzene.[7] Together with various studies on reverse micelles in different solvents (see for example Refs. 8 and 9 for AOT water in oil microemulsions) these studies suggest that the discrete nature of solvent particles plays an important role. Taking into consideration solvent–solvent and solute–solvent interactions—actually for discrete species—would then make problematic a computation of the potential of mean force according to a Hamaker's scheme. On the other hand, it becomes also difficult to understand how the solvation of the micelles, for example, would combine with other forces so as to make the attraction in the potential of mean force almost proportional to the overlap volume as in the picture of surface chains overlap accompanied with oil removal.

Therefore, it seemed to us worth reconsidering the analysis of experimental data from a truly multicomponent model of the microemulsion. Solvent–solvent, solvent–solute, and solute–solute interactions are then directly incorporated in the model. In principle, one may deal with this problem by using standard methods of the theory of liquids but in practice only approximate theories and simple models of the interactions are tractable. Indeed, recent techniques such as density functional calculations[10] or refinements of the integral equations approach[11] cannot yet cope with the combined effect of high size asymmetry and attractive forces which characterize many colloidal systems. For simplicity, we therefore considered the sticky hard-sphere model[12] (SHSM) for mixtures which admits an analytical solution[13,14] in the Percus–Yevick approximation (PYA). Despite the singular behavior of the SHSM for strictly monodisperse systems—as pointed out by Stell[15]—and the limitations of the PYA in the case of hard-sphere mixtures with high size asymmetry (see for example Ref. 11), this multicomponent SHSM—besides being the simplest model tractable at present—has proved to account fairly well for some general

 0021-9606/97/106(1)/376/12/$10.00

trends in binary mixtures of atomic fluids,[14] adsorption studies (see for example Refs. 16 and 17) and colloidal structure (see for example Refs. 18–23 and references therein). However, if one intends to go beyond the purely qualitative aspects, the application of such an already simplified approach to a specific microemulsion raises several questions about which little is known *a priori*. Besides the fact that the interaction potentials in the real system are not necessarily short ranged, one indeed needs to specify for a binary mixture at least three energetic parameters (stickiness parameters), three geometrical ones (hard-sphere radii) and a relation between the packing fractions imposed by the thermodynamic constraints (constant pressure and temperature for example).

Nevertheless, an attempt in this direction is made in this work, with a special care for the connection between the parameters of the model and the physico-chemical characteristics of the microemulsion. Complementary data to those analyzed in a preliminary report of this study[24] will also be considered. This paper is then organized as follows: In Sec. II, the main steps of the solution in the PYA of the SHSM for mixtures are recalled briefly. In Sec. III the model of the mixture is presented. The modeling of the various interactions by sticky potentials is discussed. Special attention is paid to the solvent, in order to define an appropriate equivalence between the actual interaction potential and its sticky representation. In Sec. IV, after having detailed the methodology used for analyzing the experimental data, the results are finally presented and the physical picture which emerges from a multicomponent analysis is discussed.

II. ADHESIVE SPHERES MIXTURE IN THE PERCUS–YEVICK APPROXIMATION

The main steps for computing in the PYA the structure factors for an N-component mixture of adhesive spheres are briefly recalled here (details can be found for instance in Refs. 13 and 14). Let D_k, ρ_k, and $\eta_k=(\pi/6)\rho_k D_k^3$ be respectively the hard-sphere diameter, number density, and packing fraction of the kth species. The Baxter sticky potentials $u_{mn}(r)$ between species m and n are defined by

$$\exp\left[-\frac{u_{mn}(r)}{kT}\right]=\frac{D_{mn}}{12\tau_{mn}}\,\delta(r-D_{mn})+\Theta(r-D_{mn}), \quad (1)$$

where $\delta(r-D)$ is the Dirac distribution, $\Theta(r-D)$ the unit step function, τ_{mn} the stickiness parameter, and $D_{mn}=(D_m+D_n)/2$. The adhesiveness factors λ_{mn} associated with the τ_{mn} are defined from the singular part of the direct correlation functions $c_{mn}(r)$ as

$$c_{mn}(r)=\Theta(D_{mn}-r)c_{mn}^{r}(r)+\frac{\lambda_{mn}D_mD_n}{12D_{mn}}\,\delta(r-D_{mn}), \quad (2)$$

where c_{mn}^{r} is the regular part of $c_{mn}(r)$. They are obtained from D_{mn}, τ_{mn}, and η_m by solving the system of $N(N+1)/2$ coupled quadratic equations[13,14]

$$\lambda_{mn}\frac{\tau_{mn}}{D_{mn}}=x\,\frac{D_{mn}}{D_mD_n}+\sum_{k=1}^{N}\left(\frac{\eta_k}{2D_k}\right)\left[3x^2-x(\lambda_{mk}+\lambda_{kn})+\frac{\lambda_{mk}\lambda_{kn}}{6}\right], \quad (3)$$

where $x=(1-\Sigma_{k=1}^{N}\eta_k)^{-1}$.

In Baxter's formalism, the partial structure factors S_{mn} related to the c_{mn} by the matrix equation $\mathbf{S}^{-1}=\mathbf{I}-\mathbf{C}$ are computed from the auxiliary matrix equation $\mathbf{S}^{-1}=\mathbf{Q}^{\dagger}\mathbf{Q}$. $\mathbf{Q}^{\dagger}$ is the transposed and complex conjugated of the matrix $\mathbf{Q}$ whose elements $q_{mn}(q)$ are the Fourier transforms of the Baxter's functions and depend on the coefficients λ_{mn} obtained from Eq. (3). Explicit expressions can be found for instance in Refs. 18 and 22.

Hereafter, a solute–solvent mixture ($N=2$; 1≡solvent, 2≡solute) is considered. The zero wave vector limit of the solutes structure factor, $S_{22}(0)$, can be computed from the following explicit expressions:[22,24]

$$\begin{aligned}
&S_{22}(0)=\frac{|q_{11}(0)|^2+|q_{21}(0)|^2}{|\det\,\mathbf{Q}(0)|^2},\\
&q_{11}(0)=1+\eta_1[x+(1+x\,\eta_1)\Lambda_{11}+xy\,\eta_2\Lambda_{12}],\\
&q_{21}(0)=\sqrt{y\,\eta_1\eta_2}[xy(1+\eta_2\Lambda_{22})+(1+x\,\eta_1)\Lambda_{12}],\\
&\det\,\mathbf{Q}(0)=x(1+\eta_1\Lambda_{11}+\eta_2\Lambda_{22}+\eta_1\eta_2\,\det\,\Lambda),
\end{aligned} \quad (4)$$

where $y=D_1/D_2$ is the diameter ratio, $\Lambda_{ij}=3x-\lambda_{ij}$ and det means determinant. In practice, one has to solve numerically Eqs. (3) which for $N=2$ form a set of three coupled quadratic equations for λ_{11}, λ_{12}, and λ_{22} with τ_{11}, τ_{12}, τ_{22}, η_1, η_2, and y as input parameters. Details on the numerical method we have used are given in Appendix A.

III. MODEL OF THE MICROEMULSION: RELATION BETWEEN MODEL AND MICELLAR PARAMETERS

In order to establish a connection between the physico-chemical parameters of the micromemulsion and the parameters τ_{11}, τ_{12}, τ_{22}, η_1, η_2, and y defined above, we consecutively examine the model for the solvent, the solute, and the solute–solvent coupling.

A. Representation of the solvent in the sticky hard-sphere model

Before proceeding further, the motivation of this section must be clarified: Rather than a study of the solvent per se, what we seek is a simple way of incorporating solvent hard core repulsions and attractive forces in the model of the mixture. Here, we examine how this can be done from the SHSM which indeed provides the simplest route for this purpose.

We first define the hard core diameter $D_1=[(6\,\eta_1^b)/(\pi\rho_1^b)]^{1/3}$ by fixing the value $\eta_1^b=0.4$ of the *hard core packing fraction* (ρ_1^b is the bulk number density). This value is appropriate for describing the structure of liquids at normal pressure and temperature conditions (a comparison with some results with $\eta_1^b=0.45$ will be made). This definition which ignores the complication caused by a possible

TABLE I. Influence of the depth and the range of the square well on the pseudo packing fraction and stickiness of the equivalent sticky model from Eq. (9).

		$\eta_1^b=0.45$				$\eta_1^b=0.4$			
ϵ/kT	λ	$\tilde{\eta}_1$	$\tilde{\tau}_{11}$	$S_{11}(0)$	N_c	$\tilde{\eta}_1$	$\tilde{\tau}_{11}$	$S_{11}(0)$	N_c
1.5	1.5	0.565	0.375	0.037	13.66	0.510	0.235	0.091	12.44
1	1.5	0.525	0.769	0.033	13.07	0.470	0.543	0.066	11.85
1	1.2	0.483	1.138	0.038	7.22	0.430	0.895	0.065	5.98
0.5	1.2	0.465	2.740	0.031	6.93	0.413	2.236	0.051	5.68

nonsphericity of solvent molecules—dodecane here—seems reasonable since we do not aim at a fine description of the solvent structure.

A more serious problem is the representation of the attractions. Indeed, since the range of the intermolecular potential $\phi(r)$ of ordinary solvents is comparable to the molecular size, the appropriate choice of the stickiness parameter τ_{11} should be carefully examined. In our opinion, this aspect of the SHSM has been overlooked in most of the studies of mixtures mentioned previously and relative to colloidal[18–23] but also atomic or molecular fluids.[14,16,17] Since the idea of representing relatively long ranged potential by an equivalent SHSM might thus appear somewhat provocative, we detail here the way it can be given a sensible meaning in the context of the multicomponent adhesive sphere mixture.

Because a mapping onto the SHSM of a realistic potential $\phi(r)$—especially when not short ranged—cannot of course be expected to reproduce all the associated thermodynamics, we will privilege here a mapping which best reproduces the structure. This is because we are mostly interested in the solute structure factor $S_{22}(0)$ (at zero wave number) which largely depends on the self-adhesion of the solvent.[20–22] Since this adhesion determines also the magnitude of $S_{11}(0)$, we found it important to have at least a good description of $S_{11}(0)$ for the pure solvent. For this purpose, one may think of using first the same procedure as for *thin* square wells, i.e., mapping $\phi(r)$ onto the SHSM through the equality of the second virial coefficients

$$B_2=2\pi\int_0^\infty (1-e^{-\phi(r)/kT})r^2\,dr. \tag{5}$$

The stickiness defined from the virial equivalence then reads

$$\frac{1}{\tau_v}=12\int_1^\infty (e^{-\phi(x)/kT}-1)x^2\,dx, \tag{6}$$

where x is in units of the hard-sphere diameter. Equation (6) follows from Eq. (5) which for the sticky potential gives $B_2^{\mathrm{st}}=V_{\mathrm{hs}}[4-(1/\tau)]$ where V_{hs} is the hard-sphere volume. While this procedure is acceptable for *thin* square wells at low and moderate densities[25–27] (see however the discussion in Ref. 28), it gives—at the density of liquids—much too high compressibilities (or zero wave number structure factors $S_{11}(0)=\rho_1 kT\chi_T$ in Table I above) for *wide* ones.

Therefore, a different correspondance between the SHSM and $\phi(r)$ is required. For $\phi(r)$, we may refer to the results (see for example Ref. 29 and for recent work see Refs. 28, 30 and 31) for square wells of different depths ϵ and widths $\delta_1=(\lambda-1)\sigma$ (here $\sigma\equiv D_1$). The problem now is that at packing fractions $\eta_1^b\approx 0.4$–0.45 typical of liquids packing effects prevail and the values of $S_{11}(0)$ for $\lambda\approx 1.5$ and $\epsilon/kT\approx 1$ differ only slightly from those for hard spheres (see Table I). We thus need a second criterion more sensitive to the attractions than $S_{11}(0)$. While other choices can be considered (see for instance Ref. 32 for an alternative definition of the stickiness parameter for sticky chains), we found it convenient to use the coordination number N_c defined as the number of particles in the range $\delta_1=(\lambda-1)\sigma$ around a central one

$$N_c=\int_\sigma^{\lambda\sigma}\rho_1^b g^{\mathrm{sw}}(r)4\pi r^2\,dr, \tag{7}$$

where $g^{\mathrm{sw}}(r)$ is the square well radial distribution function. For the equivalent sticky potential, $g^{\mathrm{st}}(r)=(\lambda_{11}/12)\times\delta(r-\sigma)+g^r(r)$ and we define N_c as

$$N_c^{\mathrm{st}}=2\tilde{\eta}_1\lambda_{11}+\int_\sigma^{\lambda\sigma}\tilde{\rho}_1 g^r(r)4\pi r^2\,dr. \tag{8}$$

The solvent will thus be modeled as fluid of ''pseudoadhesive'' spheres, with *pseudo packing fraction* $\tilde{\eta}_1$ and stickiness $\tilde{\tau}_{11}$ determined by two coupled equations

$$\begin{aligned} &S_{11}^{\mathrm{sw}}(0;\eta_1^b,\epsilon_{11},\sigma,\lambda)=S_{11}^{\mathrm{st}}(0;\tilde{\eta}_1,\tilde{\tau}_{11}),\\ &N_c^{\mathrm{sw}}(\eta_1^b,\epsilon_{11},\sigma,\lambda)=N_c^{\mathrm{st}}(\tilde{\eta}_1,\tilde{\tau}_{11},\lambda). \end{aligned} \tag{9}$$

In Eq. (9), $\tilde{\tau}_{11}$ and $\tilde{\eta}_1=(\pi/6)\tilde{\rho}_1\sigma^3$ are the unknowns. It must be so because if $\tilde{\eta}_1$ were equal to the hard core packing fraction $\eta_1^b=(\pi/6)\rho_1\sigma^3$, the required low values of $S_{11}(0)$ could be obtained only with τ_{11} high (equivalence *b* in Table II), which amounts to loosing the attractions present in the real system. In order to simultaneously have a non-negligible stickiness and low values of $S_{11}(0)$, the only solution is to consider a pseudopacking fraction $\tilde{\eta}_1$ different from η_1^b. The procedure consisting in defining a packing parameter different from the hard core packing fraction when computing $S_{11}(0)$ has also been adopted by Menon *et al.*[26] whom, following Baxter,[12] defined a packing fraction $\eta_1=(\pi/6)\rho_1(\lambda\sigma)^3$ which equals η_1^b only in the limit $\lambda\to 1$. The difference here is that $\tilde{\eta}_1$ is defined implicitly by Eqs. (9).

It is again stressed that Eqs. (9) merely provide a convenient way of obtaining the same values of $S_{11}(0)$ as for square wells while preserving the effect of the attractions

TABLE II. Comparison of different definitions of the equivalent sticky for the wells SW1 and SW2. (a) Same $S_{11}(0)$ and coordination number N_c [Eq. (9)]; (b) same $S_{11}(0)$ and $\tilde{\eta}_1=0.4$; (c) same $S_{11}(0)$ and $[-U/(N\epsilon)]_{sw}=\tilde{\eta}_1\lambda_{11}$; (d) same second virial coefficient and $\tilde{\eta}_1=0.4$.

	SW1: $\epsilon/kT=1.5$, $\lambda=1.5$				SW2: $\epsilon/kT=0.5$, $\lambda=1.2$			
	$\tilde{\eta}_1$	$\tilde{\tau}_{11}$	$S_{11}(0)$	N_c	$\tilde{\eta}_1$	$\tilde{\tau}_{11}$	$S_{11}(0)$	N_c
(a)	0.510	0.235	0.091	12.44	0.413	2.236	0.051	5.68
(b)	0.4	0.741	0.091	10.22	0.4	3.32	0.051	5.35
(c)	0.73	0.01	0.091	12.44	0.558	0.260	0.051	5.68
(d)	0.4	0.0302	272	10.61	0.4	0.529	0.113	5.42

through the coordination number and do not constitute a full mapping. Besides to leading to an obviously different structure in real space (see Fig. 1), an example which shows that this procedure certainly does not reproduce all the thermodynamics associated with the square well is the configurational internal energy per particle U/N related to N_c^{sw} by $[-U/(N\epsilon)]_{sw}=N_c^{sw}/2$ and whose sticky limit is $[-U/(N\epsilon)]_{st}=\tilde{\eta}_1\lambda_{11}$. Since our definition of N_c^{st} includes the contribution of the regular part of $g^{st}(r)$, $\tilde{\eta}_1\lambda_{11}$ is not equal to $[-U/(N\epsilon)]_{sw}$. The reason for having privileged the coordination number is that imposing $[-U/(N\epsilon)]_{sw}=\tilde{\eta}_1\lambda_{11}$ would have required an exceedingly high stickiness (equivalence c in Table II).

Table I shows some results for $\tilde{\tau}_{11}$ and $\tilde{\eta}_1$ from Eq. (9). Since computer simulations results [especially for $S_{11}(0)$] are not available for all the wells in Table I, N_c^{sw} was computed from the mean spherical approximation (MSA) for $g^{sw}(r)$, which for $\eta_1^b\approx0.4$ gives satisfactory results for not too deep and narrow wells.[29] For each well, $\tilde{\tau}_{11}$ and $\tilde{\eta}_1$ are varied until Eq. (9) is satisfied, the right-hand side being computed with the MSA, λ_{11} and $S_{11}(q)$ from standard relations[12] followed by numerical integration for $g^r(r)$ and N_c^{st}.

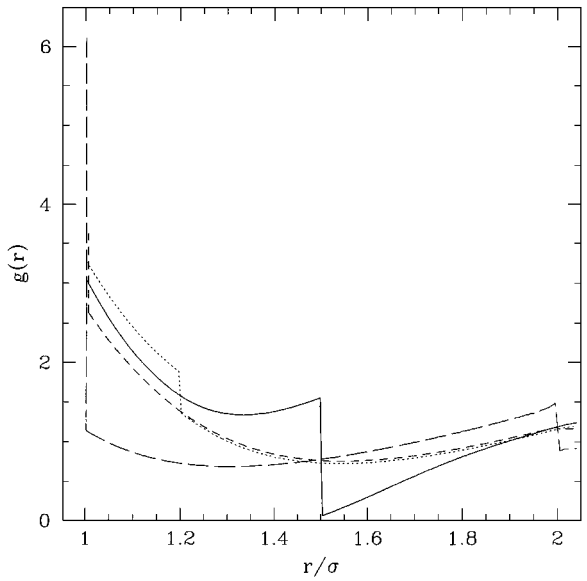

FIG. 1. Comparison of the radial distributions functions for square wells and the equivalent SHSM from Eqs. (9). SW1:MSA full curve, SHSM: Long dashed curve; SW2:MSA dotted curve, SHSM: Short dashed curve. For the SHSM, the length $2\tilde{\eta}_1\lambda_{11}$ of the vertical lines is equal to $\int_\sigma^{\lambda\sigma}4\pi r^2[\rho_1 g^{sw}(r)-\tilde{\rho}_1 g^r(r)]dr$.

Two main features can be noticed for the wells in Table I: N_c depends mostly on the range and for the same range, $S_{11}(0)$ increases slightly with the depth. We will thus consider in the rest of this work the two extreme cases: A deep and wide well ($\epsilon/kT=1.5$, $\lambda=1.5$) hereafter labeled SW1 and a relatively shallow and narrow one ($\epsilon/kT=0.5$, $\lambda=1.2$) labeled SW2, both for $\eta_1^b=0.4$. While with $\eta_1^b=0.45$ no essential difference was found, $\eta_1^b=0.4$ gives lower values of $\tilde{\eta}_1$ which is preferable for reasons discussed in Sec. III C.

In what concerns the relation with experiment, it should be noted that although SW1 is rather deep and wide, the magnitude of the associated B_2 is much lower than what can be estimated for dodecane from empirical formulae[33] (as an example, with the method of Ref. 33(a) we obtained $B_2^{exp}\approx-12000$ cm^3 mol^{-1} at 300 K). With $\eta_1^b=0.4$ and a molecular volume $v_d\approx378$ Å^3 we have $V_{HS}\approx151$ Å^3. Assuming $\lambda=1.5$, the required depth is $\epsilon=2.73$ kT, leading to $S_{11}(0)\approx0.5$ and $N_c\approx13.8$ in the MSA. Although the MSA becomes less accurate for large values of ϵ/kT, for such values of $S_{11}(0)$ and N_c the equivalent sticky would correspond to so low values of $\tilde{\tau}_{11}$ that even the existence of a liquid phase would be questionable (see Ref. 34 for this point). It is actually difficult to say that an isotropic potential with parameters deduced from B_2^{exp} is a realistic representation for a long linear alkane as dodecane. Other possibilities have been discussed for instance in Ref. 35. For all these reasons, we have not retained these square well parameters. By using SW1 and SW2 we should thus obtain indications on the sensitivity of the model to the solvent intermolecular potential rather than results which can be interpreted as pertaining strictly to dodecane.

We finally conclude this section by comparing in Table II different ways of defining an equivalent sticky for SW1 and SW2. The first three give the same $S_{11}(0)$ and the last one is the virial equivalence. The square well radial distribution functions and those of the SHSM defined by Eq. (9) are shown in Fig. 1 mostly for illustrating the importance of the contribution of $g^r(r)$ in the computation of N_c^{st}. We may notice that the virial equivalence (d) gives as expected meaningless values of $S_{11}(0)$ for SW1. Since the values of N_c are then lower than for the square well, an alternative equivalence keeping η_1^b but imposing N_c would lead to even

TABLE III. Micellar parameters. R^{ap}: Apparent radius in nm. B_2': twice the osmotic second virial coefficient in units of the apparent micellar volume $v_m=\frac{4}{3}\pi R^{ap3}$. Δn_c: difference in number of CH groups between surfactant and alcohol. ρ_1^b: solvent average bulk number density in nm^{-3}. D_2/D_1: Solute–solvent hard-sphere diameter ratio. Surfactants: Sodium dodecylsulfate (SDS) (C_6^1, C_6^2, C_7^a) and methyl-SDS (C_7^b) alcohols: Hexanol (C_6^1, C_6^2) and heptanol (C_7^a, C_7^b).

	C_6^2	C_6^1	C_7^a	C_7^b
R^{ap}	6.3±0.5	4.8±1	6.1±0.2	6.0
B_2'	−3.8±1	−1.5±0.5	+3±2	−4
Δn_c	6	6	5	6
ρ_1^b	2.919	2.898	2.864	2.793
D_2/D_1	17.34	12.61	17.0	16.6

less acceptable results. Equivalence (b) would be acceptable but it leads to lower values of N_c (the values are even worse with $\eta_1^b=0.45$). The associated stickiness is also relatively low and would underestimate the energetic contribution of solvent–solvent attractive forces which are of particular importance in the mixture[20–22]). Equivalence (c) gives both high values of $\tilde{\eta}_1$ and very high stickinesses. With SW2 the four routes converge towards similar results as expected. For these reasons, we have privileged the equivalence defined by Eq. (9). Its consequences for the mixture will be examined in Sec. IV A.

B. Model of the reverse micelles

This model concerns the reverse micelles investigated by Brunetti *et al.*[1] The parameters of the selected micelles are given in Table III. These micelles have an aqueous core and a surface layer made of a surfactant which is sodium dodecylsulfate (SDS) for C_6^2, C_6^1, and C_7^a,[1] and methyl-SDS for C_7^b [3] and an alcohol, either hexanol (C_6^2, C_6^1), or heptanol (C_7^a, C_7^b). It is usually admitted that the impenetrable core (of radius R^{hs}) extends up to the end of the alcohol chains. The region from the end of the alcohol chains up to the end of the surfactant chains forms a penetrable shell of thickness $l\Delta n_c$ (see Fig. 2). Δn_c is the difference in the number of CH groups between surfactant and alcohol (assuming the chains to be in extended conformation, $l=0.126$ nm). The volume of this shell changes with the interpenetration length $l\Delta n_c$ for micelles of same size (C_7^a, C_6^2, and C_7^b), and with the micellar radius R^{ap} at constant Δn_c (C_6^2 and C_6^1).

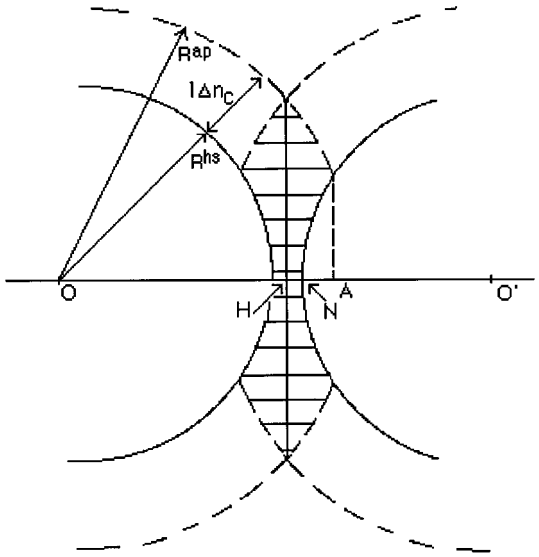

FIG. 2. Schematic representation of two interpenetrating micelles. The overlap volume of two micelles corresponds to the common (shaded) part of the penetrable shells of thickness $l\Delta n_c$ between the hard sphere of radius R^{hs} (end of alcohol chains) and the outer sphere of radius R^{ap} (end of surfactant chains).

From the apparent diameter D_2^{ap} and following Ref. 1, we define the micelles hard-sphere diameter as $D_2=D_2^{ap}-2l\Delta n_c$. Our model of the intermicellar interaction potential $U_{22}(r)$ consists thus of a hard-sphere repulsion for a center to center micellar separation $r\leqslant D_2$ and an attractive part assumed proportional to the overlap volume $V^o(r)$ (shaded region in Fig. 2): $U_{22}^{at}(r)=\alpha V^o(r)$. From the intermicellar distance $r=OO'$ (Fig. 2) and the distances $AH=[1/2r](R^{ap^2}-R^{hs^2})$ and $AN=R^{hs}+[1/2r]\times(R^{ap^2}-R^{hs^2}-r^2)$, $V^o(r)$ can be computed as

$$V^o(r)=\begin{cases} 2\pi\left[AHR^{ap^2}-\frac{1}{3}\left(AH+\frac{r}{2}\right)^3-\left(\frac{r}{2}\right)^3\right]-2\pi\left(R^{hs}AN^2-\frac{1}{3}AN^3\right); & D_2\leqslant r\leqslant R^{hs}+R^{ap} \\ \frac{\pi}{6}(D_2^{ap}-r)^2\left(D_2^{ap}+\frac{r}{2}\right); & R^{hs}+R^{ap}\leqslant r\leqslant D^{ap} \\ 0; \quad r<D_2, \quad r\geqslant D^{ap} \end{cases} . \tag{10}$$

This overlap volume is smaller than that defined in our previous work[24(a)] (middle term of Eq. (10) with $D_2\leqslant r\leqslant D^{ap}$) since the region $r<D_2$ is now trully impenetrable (we could have computed a more realistic repulsive contribution by using the arguments of Lemaire *et al.*[2] on volume restriction effects, but we found this complication incommensurate with the simplicity of the model for the attractive one).

In this picture, $U_{22}^{at}(r)$ is assumed to arize from the van der Waals interaction between CH groups of surfactants when the surface layers of two approaching micelles interpenetrate. α is a proportionality constant related to the average of this interaction in the overlap volume and in the pres-

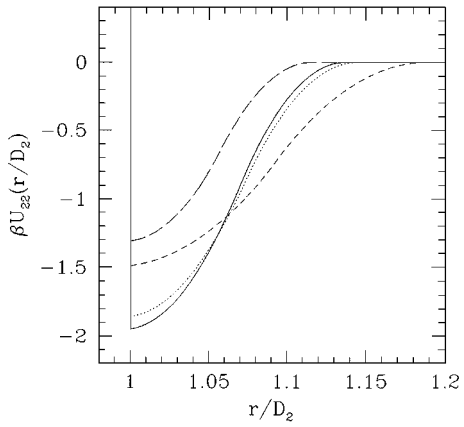

FIG. 3. Overlap potential vs reduced distance. Full curve: C_6^2; dotted curve: C_7^b, short dashed curve: C_6^1; long dashed: C_7^a. The energetic constant α is such that the equivalent stickiness parameter for C_6^2 is $\tau_{22}^{eq}=0.25$.

ence of the solvent. A computation of this average from the parameters of the van der Waals interaction between CH groups requires a detailed knowledge of the organization of the surfactant and solvent at the interface (In Ref. 2, the pair correlation function of CH groups was taken as a purely radial one, equal to unity outside the hard cores). Since this would be an involved task, α will be taken here as one free parameter of the model. If the chain length of surfactant and/or cosurfactant is changed only slightly, a major reorganization of surfactant or solvent is not expected, so that keeping α constant when the same solvent is considered should be a reasonable assumption.

In order to map this potential onto the SHSM, we used the virial equivalence defined by Eqs. (5) and (6) since—in contrast with the situation for the solvent—$U_{22}(r)$ is now short ranged and the micellar packing fractions lower. For each value of τ_{22}, α is determined by solving numerically Eq. (6). An illustration is given in Fig. 3. We first observe that the longer range (in reduced units) is that of the smallest micelle (C_6^1) and is less than 0.2. The values at contact of $U_{22}(r/D_2)$ for C_6^2 and C_7^b are nearly equal since they have the same $\Delta n_c=6$ and nearly the same radius (for C_7^b both the alcohol and surfactant are longer by one CH_2 unit). $|U_{22}(r/D_2)|$ is significantly lower for C_7^a because of the extra CH_2 unit of heptanol which reduces the interpenetration length by 0.126 nm. The intermediate position of C_6^1 for which $\Delta n_c=6$ is due to its smaller radius. Since α is unknown, we cannot specify the actual magnitude of U_{22}. It is however interesting to notice that $|U_{22}(1)|$ is slightly lower than the value at the minimum of the potential of mean force (about 2.5 kT for the micelles C_6 for example) of Ref. 2. For reasons discussed in Sec. IV A, we will thus consider a series of values of α leading to values of τ_{22}^{-1} for C_6^2 between 1 and 6 and spaced by one unit ($0.1666 \leqslant \tau_{22} \leqslant 1$), and corresponding to $0.83 \leqslant \beta U_{22}(r/D_2) \leqslant 2.36$. The equivalent stickiness coefficients τ_{22}^{eq} for the other micelles are given in Table IV.

We may finally notice that as in Ref. 2, other contributions to the micellar interaction such as the van der Waals interaction between the water cores or electrostatic

TABLE IV. Stickiness parameter τ_{22}^{eq} determined from the overlap potential. The values of the constant $\alpha_0=[\pi/(6kT)]\alpha D_2^3$ are for C_6^2 and correspond via the virial equivalence for the overlap potential to the series of values of τ_{22}^{eq} in the second column.

α_0	$\tau_{22}^{eq}(C_6^2)$	$\tau_{22}^{eq}(C_6^1)$	$\tau_{22}^{eq}(C_7^a)$	$\tau_{22}^{eq}(C_7^b)$
148.30	0.166	0.210	0.439	0.175
136.50	0.20	0.244	0.507	0.187
122.55	0.25	0.295	0.606	0.259
105.40	0.333	0.378	0.766	0.343
83.20	0.5	0.540	1.079	0.509
51.93	1.0	1.017	1.990	1.007

interactions[36] are not considered here. This is equivalent to assuming that—if non-negligible compared with the chain overlap interaction—these contributions do not change significantly for the micelles investigated here.

C. Micelle–solvent coupling

This coupling involves two main aspects. The first one concerns the solvent–micelle interaction $U_{12}(r)$. Little is actually known on this interaction but what is needed in our method is its change with the nature of the micelle. We thus considered standard representations[16,17] that is a hard-sphere repulsion for $r<D_{12}$ plus either a square or a triangular well $U_{12}^{at}(r)$ of depth ϵ_{12} both with a range $\Delta_{12}=0.5D_1$. The triangular well is defined by

$$U_{12}^{at}(r)=\frac{\epsilon_{12}}{\Delta_{12}}\,(r-\Delta_{12}-D_{12}); \quad D_{12}\leqslant r\leqslant \Delta_{12}+D_{12}. \tag{11}$$

$D_{12}=(D_1+D_2)/2$ being the mean hard-sphere diameter. The associated stickiness parameter from the virial equivalence [Eq. (6)] reads

$$\frac{1}{\tau_{12}}=4(e^{\beta\epsilon_{12}}-1)(\delta_{12}^3-1), \quad \text{(square)}, \tag{12a}$$

$$\frac{1}{\tau_{12}}=12\left\{\epsilon_r^{-3}\,\exp(-\epsilon_r\delta_{12})[f(\epsilon_r\delta_{12})-f(\epsilon_r)] - \frac{1}{3}\,(\delta_{12}^3-1)\right\} \quad \text{(triangular)}, \tag{12b}$$

where

$$\delta_{12}=1+\frac{\Delta_{12}}{D_{12}}, \quad \epsilon_r=-\frac{\beta\epsilon_{12}}{(\delta_{12}-1)}$$

and

$$f(u)=e^u(u^2-2u+2).$$

For micelles in the same solvent, the simplest assumption is to consider that ϵ_{12} and Δ_{12} are unchanged when the micellar surface layers are of same chemical composition and nearly same structure (see Sec. IV C). As shown in the next section, the fits to experiment can be used to test this assumption.

The second aspect of the solvent–micelle coupling is that in constant pressure experiments, the packing fractions η_1 and η_2 are not independent variables. In order to impose a

realistic pressure, we need a reliable equation of state for the mixture and none is available for large size asymmetry. We nevertheless tried the pressure $p_c^{\mathrm{PY}}(\eta_1,\eta_2)$ obtained from the Percus–Yevick compressibility equation for the mixture.[14] η_1 can then be determined from the fixed pressure p_0 and η_2 by solving $p_c^{\mathrm{PY}}(\eta_1,\eta_2)=p_0$. But here again we face the problem of the incomplete mapping of wide potentials onto the SHSM. In particular, with a reasonable estimation of the solvent particles diameter and a moderate stickiness, the solvent pressure is too high compared to that computed with wide square wells. Since it is a large contribution to the total pressure, $p_c^{\mathrm{PY}}(\eta_1,\eta_2)$ is then too high. With SW1 for example, the MSA pressure for the pure solvent is negative, while the SHSM pressure is $p_c^{\mathrm{PY}}(.51,\eta_2\to 0)=411$ atm ($D_1=0.64$ nm), the hard-sphere contribution being $p_{\mathrm{hs}}^{\mathrm{PY}}=2172$ atm. If this contribution is computed from the more accurate Carnahan–Starling expression[37] we have $p_{\mathrm{hs}}^{\mathrm{CS}}=2009$ atm. This shows that even in the SHSM, the magnitude of the pressure $p_c^{\mathrm{PY}}(\eta_1,\eta_2)$ is questionable. Even at high η_2 the solvent contributions (hard sphere and attractive) are still large. For example $p_c^{\mathrm{PY}}(0.33,0.3)=329$ atm results largely from the reduction of the total hard-sphere contribution $p_{\mathrm{hs}}^{\mathrm{PY}}=1650$ atm by a contribution of -1240 atm depending only on the adhesiveness coefficient λ_{11}. The limited accuracy of the PY compressibility pressure together with the inadequacy of the SHSM for reproducing the much lower pressures of wide square wells led us to not proceed with constant pressure calculations. Since we are more concerned in this work with the structure than with the pressure itself, we found it simpler to keep constant the packing fraction $\eta_1/(1-\eta_2)$ of the small particles relative to the free volume left by the large ones. As for binary mixtures of hard spheres,[11] this is roughly equivalent to keeping constant $p_c^{\mathrm{PY}}(\eta_1,\eta_2)$ (in the example shown above the variation from the pure solvent to the mixture with $\eta_1=0.3$ is about 20% of the average value). η_1 was thus determined as $\eta_1=\tilde{\eta}_1(1-\eta_2)$. The solvent relative packing fraction being taken equal to the pseudopacking fraction $\tilde{\eta}_1$, the solvent contribution to the pressure is roughly constant. This will however have an incidence in the mixture when $\tilde{\eta}_1$ differs from η_1^b. A measure of this is the areal packing fraction

$$\theta_{12}^s=\frac{N_{12}^{\mathrm{ads}}}{S}\,\frac{\pi D_1^2}{4},$$

where

$$N_{12}^{\mathrm{ads}}=\rho_1\int_0^\infty \lambda_{12}\,\frac{D_1D_2}{12D_{12}}\,\delta(r-D_{12})4\pi r^2dr$$

is the number of solvent particles adsorbed on a micelle and $S=4\pi D_{12}^2$ the surface of the sphere of closest approach. This areal packing fraction reads

$$\theta_{12}^s=\eta_1\,\frac{\lambda_{12}}{4(1+y)}. \tag{13}$$

Since $\eta_1=\tilde{\eta}_1(1-\eta_2)$ and because of the implicit dependence of λ_{12} on η_1, $\tilde{\eta}_1$ should not differ too much from η_1^b for θ_{12}^s being not too different from the real areal packing fraction. This is the reason for prefering $\eta_1^b=0.4$ which indeed leads to lower values of $\tilde{\eta}_1$ than $\eta_1^b=0.45$. Except for leading to this difficulty in the interpretation of θ_{12}^s, it is stressed than the precise choice of $\tilde{\eta}_1$ has no incidence on the main conclusions of this work.

Having defined the connection with model and micellar parameters, we are now in the position to proceed with the analysis of experimental data.

IV. RESULTS AND DISCUSSION

A. Methodology

The data that will be analyzed in this section are solute structure factors deduced from light scattering measurements.[1] Since only the intensities were given, the ''experimental'' values of $S_{22}(0)$ were computed from Vrij's formula which reproduces very well the original data.[1] Experimental volume fractions ϕ are converted into hard-sphere packing fractions as $\eta_2=\phi(D_2/D_2^{\mathrm{ap}})^3$. In order to compute the theoretical $S_{22}(0)$, we must specify four free parameters: $\tilde{\eta}_1$ and $\tilde{\tau}_{11}$ for the solvent, α (or τ_{22}) for the micelles and τ_{12} for the solvent–micelle coupling. For $\tilde{\eta}_1$ and $\tilde{\tau}_{11}$, the couples ($\tilde{\eta}_1=0.51$; $\tilde{\tau}_{11}=0.235$) (SW1) and ($\tilde{\eta}_1=0.413$; $\tilde{\tau}_{11}=2.236$) (SW2) were used. As a check we have also considered ($\tilde{\eta}_1=0.4$; $\tilde{\tau}_{11}=0.741$) [equivalence (b) for SW1]. The strategy adopted for the other parameters is illustrated below in a diagrammatic way for the micelles C_6^2 and C_6^1.

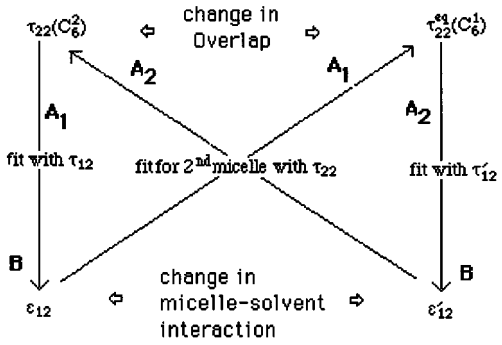

Paths A corresponds to the assumption of a constant solvent–micelle interaction $U_{12}(r)$. For each couple $(\tilde{\eta}_1;\tilde{\tau}_{11})$ we start with a value of τ_{22} for the micelle C_6^2 (A_1 and A_2 being symmetrical, we always used C_6^2 as the reference micelle). The theoretical $S_{22}(0)$ from Eq. (3) is then fitted to experiment for C_6^2 with the aid of τ_{12}. From τ_{12} and Eq. (12), the depth ϵ_{12} is obtained for the triangular or square well of range $\Delta_{12}=0.5D_1$. From ϵ_{12}, a new τ_{12} is computed from Eq. (12) with the geometry of C_6^1. We finally determine the new value τ_{22}^f which fits the data for this micelle. This value is then compared with τ_{22}^{eq} obtained from the overlap potential $U_{22}(r)$. As a result, one may predict the change in intermicellar adhesion under the assumption of a constant micelle–solvent interaction.

In paths B, the data for two micelles are fitted independently with the aid of τ_{12} and by using the respective τ_{22}^{eq} computed from the overlap potentials with the same α (only the geometry changes). The well depths corresponding to the

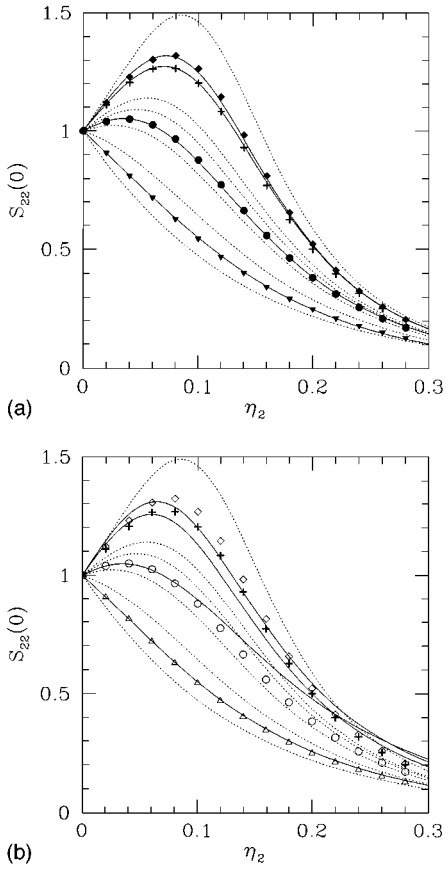

FIG. 4. Theoretical and experimental solute structure factor at zero wave number, $S_{22}(0)$ vs packing fraction η_2. [solvent well SW1 in Fig. 4(a) and SW2 in Fig. 4(b)] Theoretical: full curves. Experimental: Triangle: C_7^a, circles: C_6^1; crosses: C_6^2, diamonds: C_7^b. The two dotted curves enveloping each set of experimental points correspond to $S_{22}(0)$ computed from Vrij's formula, with account of experimental error (Ref. 1) in the osmotic virial coefficient.

two values of τ_{12} are computed from Eq. (12). We may then compare the change in the micelle–solvent interaction under the assumption that the intermicellar interaction is due to overlap.

Before discussing the main results, some general features should be mentioned.

(i) Good fits of $S_{22}(0)$, especially at high η_2 could not be obtained unless τ_{12} is allowed to vary with η_2. The typical fits obtained in path A_1 and shown in Fig. 4 were obtained with a linear decrease of τ_{12} between τ_{12}^s (for $\eta_2=10^{-5}$) and τ_{12}^m (for $\eta_2=0.3$), used as the fitting parameters (the depth of the triangular well used for passing from C_6^2 to the other micelles increases almost linearly with η_2). This increase of the hetero-stickiness with η_2 is necessary for reproducing the drop of the experimental $S_{22}(0)$ at large η_2 (the calculation were made up to $\eta_2=0.3$ while the maximum experimental volume fraction is $\phi=0.3$, which corresponds roughly to $\eta_2=0.2$ for C_6^2). The technical reason for this increase is the fact that the packing fraction $\eta_1=\tilde{\eta}_1(1-\eta_2)$ decreases with η_2. Were τ_{12} fixed, the surface coverage of the micelles should thus decrease with η_2 and a drop of a theoretical $S_{22}(0)$ would be impossible. Attempts to simulate this drop by imposing a linear increase of τ_{22} with η_2—at fixed τ_{12}—generated unsatisfactory fits. For the moment it is not possible to determine whether this necessary decrease of τ_{12} with η_2 is an artifact of the model (the PYA might underestimate solute–solvent correlations at high size asymmetry) or this corresponds to some real physical effect (in Ref. 9 the decrease in the effective stickiness of AOT–water–oil micelles was interpreted from a depletion model). This is however of no consequence in path A since apart from the geometrical dependence of τ_{12} on the diameters, the well itself is unchanged from one micelle to the other. In path B, this amount to assuming that the mechanism by which the well changes with η_2 operates similarly for the two micelles under comparison.

(ii) Relatively low values of τ_{11}, τ_{22}, and τ_{12} are needed for having acceptable fits. It can be observed that the fits with SW1 [Fig. 4(a)] are of better quality that those with SW2 [Fig. 4(b)]. This has been observed for all the values of τ_{22} we have explored. The fact that the best fits are usually obtained for rather low τ_{11} suggests that for dodecane, the well $\epsilon/kT=1.5$; $\lambda=1.5$ is more appropriate. Rather low values of τ_{22} are also required. The best fits are obtained for τ_{22} roughly in the range $0.2\leqslant\tau_{22}\leqslant0.5$. Below 0.2 the quality of the fits deteriorates significantly and above 0.5, a steep variation of the well depth ϵ_{12} with η_2 is required for reproducing the drop of $S_{22}(0)$ (see below the discussion for $\tau_{22}\to\infty$). On the other hand, obtaining better fits with low values of τ_{22} reduces some of the uncertainties related to the PYA as discussed in Appendix B.

(iii) Within these ranges, fits of comparable quality can be obtained for a series of values of τ_{11} and τ_{22}. These parameters cannot thus be obtained from the fits. The discussion will thus be made with SW1 and SW2 and for the series of values of τ_{22} for C_6^2 shown in Table IV (several checks at intermediate values generated the same trends).

B. Change in effective adhesion and change in overlap potential

Figure 5 shows the results obtained according to path A. The stickiness parameter τ_{22}^f deduced from the fits is compared to that obtained from the overlap potential τ_{22}^{eq} (for clarity of the display we show the quantities $1/\tau^*=(1/\tau_{22})+4[(D^{\mathrm{ap}}/D_2)^3-1]$ which for the same micelle merely shifts the origin of the axes). Optimum fits as those presented in Fig. 4 were obtained starting with the initial values $\tau_{22}^f=\tau_{22}^{\mathrm{eq}}$ for C_6^2 (crosses on the straight line). For the three other micelles, we observe an excellent correlation between τ_{22}^f and τ_{22}^{eq}. For C_7^a and C_7^b, the points are always close to the equality line. Independently of the actual adhesiveness of the reference micelle C_6^2, its change for the other ones is then essentially due to the change in overlap volume, the less adhesive one (C_7^a) having the shortest interpenetration length (see also Fig. 3). In a preliminary report of this work,[24(a)] we observed that for the micelles C_7^a and C_7^b, the correlation between τ_{22}^f and τ_{22}^{eq}, was less good when the solvent stickiness is high. However, the effective micellar adhesion was then mostly that induced by a highly adhesive

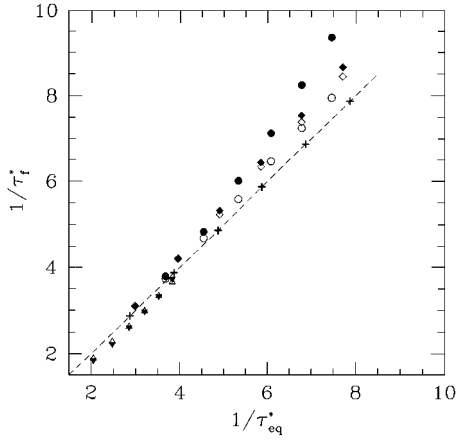

FIG. 5. Correlation between the micelles stickiness parameter deduced from the fits to experiment (τ_{22}^f) and from the overlap potential (τ_{22}^{eq}). Triangles: C_7^a, circles: C_6^1; crosses: C_6^2, diamonds: C_7^b. Solid symbols: Solvent well SW1, open symbols: SW2. τ^* is defined from τ_{22}^f and τ_{22}^{eq} by $1/\tau^*=(1/\tau_{22})+4[(D^{ap}/D_2)^3-1]$.

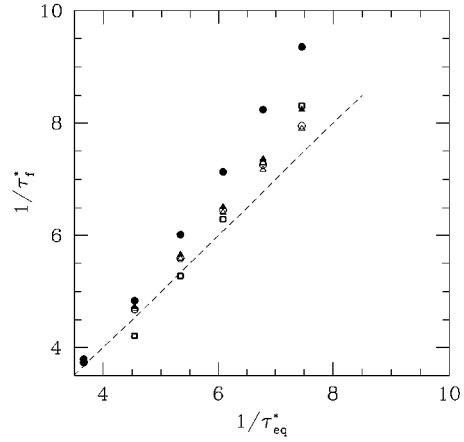

FIG. 7. Influence of the definition of the equivalent sticky on the correlation between τ_{22}^f and τ_{22}^{eq} for the micelle C_6^1. Equivalence (a): Solid circles: SW1, open circles: SW2; equivalence (b): solid triangles: SW1, open triangles: SW2. The open squares are from equivalence (a) for SW1 with correction for τ_{22}^f as explained in Appendix B.

solvent. The values $\eta_1^b=0.45$ and $\tau_{11}=0.09$ used indeed correspond to an exceedingly high $S_{11}(0)$ (the equivalent well would have an unrealisticly narrow width). A detailed discussion is made in Sec. IV C below for the smallest micelle C_6^1.

As an additional check we finally considered the micelle C_5^2 (with pentanol as cosurfactant: $\Delta n_c=7$) for which a dramatic change from C_6^2 was observed.[1] The parameters $B_2'/v_m=-27\pm3$, $R^{ap}=6.2\pm0.7$ nm for C_5^2 were determined from interpolation at infinite dilution since $S_{22}(q)$ depends on the scattering angle in the high concentration range.[1] The corresponding values for C_6^2 are $B_2'/v_m=-4.4$, $R^{ap}=6.4$ nm. In the low concentration range, the experimental values can be retrieved from the osmotic virial-coefficient as $S_{22}^{-1}(0)=1+B_2'\phi$. Figure 6 shows the corresponding results. For C_6^2 the theoretical curve was computed with SW1, $\tau_{22}^{eq}=0.25$ ($\alpha_0=128.5$), $\tau_{12}=1.553$ for the whole η_2 range. The curves for C_5^2 were computed by using the mean value $B_2'/v_m=-27$, with $R^{ap}=5.5$, 6.2, and 6.9 nm, and with the respective values $\tau_{22}^{eq}=0.109$, 0.0948, and 0.0812. We observe that the experimental points are between the theoretical curves computed with the two largest values of R^{ap}. We conclude that when the apparent radii are not significantly different, the change in effective adhesion—even if very large—can be attributed essentially to the change in overlap. As for the micelle C_6^1 ($\Delta R^{ap}\approx1.5$ nm) the results with the smallest value of R^{ap} ($\Delta R^{ap}\approx0.9$ nm) suggest that a simultaneous change in the micelle–solvent interaction should be considered. We examine this now on the example of C_6^1.

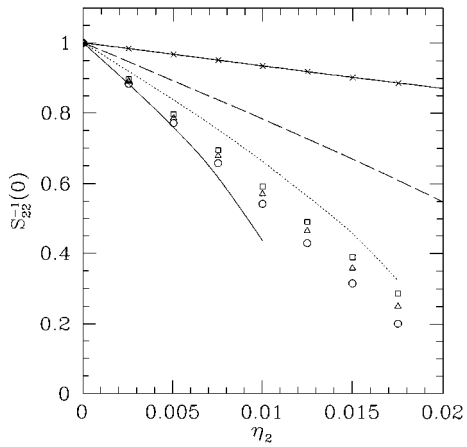

FIG. 6. Comparison of the structure factors for C_6^2 and C_5^2 in the low concentration range. C_6^2: Full curves (theory) and crosses (experiment). C_5^2: Full curve (theory) and circles (experiment) for $R^{ap}=6.9$ nm; dotted curve (theory) and triangles (experiment) for $R^{ap}=6.2$ nm; dashed curve (theory) and squares (experiment) for $R^{ap}=5.5$ nm.

C. Change in solvent–micelle interaction

For C_6^1, τ_{22}^f is lower than τ_{22}^{eq}, especially with SW1. In order to find a possible explanation, we first considered equivalence (b) for the solvent parameters ($\tilde{\eta}_1=0.4$) (see Table II). The results are shown in Fig. 7. With SW2, the results are nearly indistinguishable from those obtained from equivalence (a) ($\tilde{\eta}_1=0.51$) while for SW1, the results get closer to the line of unit slope. However, the fits of $S_{22}(0)$ are of less good quality than those with $\tilde{\eta}_1=0.51$, suggesting again that equivalence (a) from Eq. (9) should be preferred.

We have also followed path B in order to determine whether a change in ϵ_{12} might be the actual reason. In this path, the values τ_{22}^{eq} obtained from the overlap potentials are used. The results for SW1 with equivalence (a) are given in Fig. 8, for the triangular and the square well model of $U_{12}(r)$. The maximum decrease of ϵ_{12} from C_6^2 to C_6^1 is less than 4%, that is very weak. A physical basis for this change of ϵ_{12} might be to consider this quantity as the average over the micellar surface of the magnitude of the local interaction of one solvent molecule with a few surfactant and/or alcohol units. A precise estimation of this magnitude is difficult but a rough idea of its change from C_6^2 to C_6^1 can be formed by considering the change in surfactant and alcohol surface con-

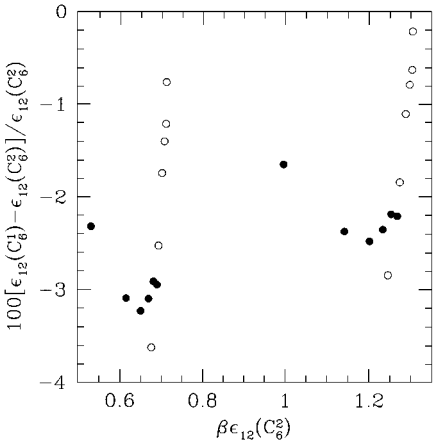

FIG. 8. Relative change in the micelle–solvent well depth from C_6^2 to C_6^1. Solid circles: ϵ_{12}^m corresponding to τ_{12}^s, open circles: ϵ_{12}^s corresponding to τ_{12}^m. Left set: Square well, right set: Triangular well. In each set and for both symbols, the self-stickiness of the reference micelle C_6^2 increases from right to left (values of τ_{22}^{eq} in Table IV).

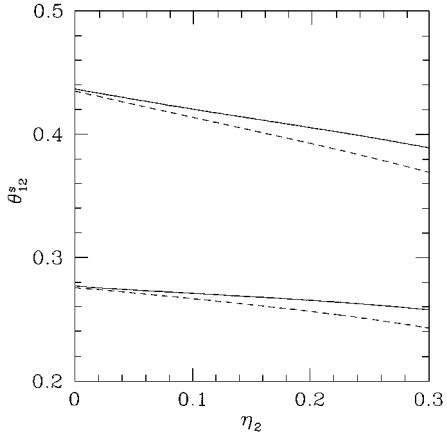

FIG. 9. Solvent areal packing fraction vs micellar packing fraction η_2 for C_6^2 and C_6^1. Full curves: C_6^2, dashed curves: C_6^1. upper curves: SW1 with equivalence (a) with $\tau_{22}^f=0.2(C_6^2)$ and $\tau_{22}^f=0.18(C_6^1)$; lower curves: SW1 with equivalence (b) with $\tau_{22}^f=0.2(C_6^2)$ and $\tau_{22}^f=0.214(C_6^1)$.

centrations. In Table I of Ref. 1 the volume composition of the microemulsions are given. From the apparent micellar volume v_m, the total volumes (for 100 cm^3 of solution) of SDS and dodecane, V_s, V_d, and the molecular alcohol/dodecane ratio A/D, one may estimate the number of SDS units per micelle as $N_s^{(m)}=v_m v_s^{-1}V_s/[100-V_d-V_a^c]$ where $V_a^c=V_d[(A/D)(v_a/v_d)]$ is the volume of alcohol in the continuous phase (v_a, v_s, and v_d being the alcohol, surfactant, and dodecane molecular volumes). We can then estimate the surfactant coverage per unit area on the sphere of closest approach as $c_S=N_s^{(m)}/(4\pi D_{12}^2)$. We thus find $c_S(C_6^1)\approx 0.92c_S(C_6^2)$. The same estimation for the alcohol gives $c_A(C_6^1)\approx 0.87c_A(C_6^2)$. This lowering of the surfactant and alcohol coverages from C_6^2 to C_6^1 corroborates a decrease of ϵ_{12} from C_6^2 to C_6^1. Since a small change in ϵ_{12} can have a large effect, one may thus think that the change in $U_{12}(r)$ might alone explain the experimental change in $S_{22}(0)$. In order to check this possibility, we have tried fits with $\tau_{22}=\infty$ (the micelles are pure hard spheres). As mentioned previously, the fits are then of even poorer quality than for $\tau_{22}\approx 1$. In addition, an extreme variation of τ_{12} with η_2 is necessary. For C_6^2 and with SW1 for example, ϵ_{12} increases from 0.174 kT ($\tau_{12}=16$) to 3.68 kT ($\tau_{12}=0.1$) for $\eta_2=10^{-5}$ and $\eta_2=0.26$ (no solutions are found beyond this value). Despite the decrease of η_1 with η_2, the associated solvent areal packing fraction θ_{12}^s increases from 0.1 to 0.34 (for C_6^1, ϵ_{12} increases from 0.24 to 3.36 kT and θ_{12}^s from 0.135 to 0.37). Besides the poor quality of the fits, it is difficult to imagine a physical mechanism which would explain such a strong micelle–solvent interaction only in concentrated microemulsions. Therefore, the assumption of a moderate change of ϵ_{12} seems indeed the most plausible.

As a final illustration of the effect of the micelle–solvent interaction we give in Fig. 9, the areal packing fraction θ_{12}^s obtained with SW1 (the triangular well U_{12} is used when going from C_6^2 to C_6^1). One may notice that θ_{12}^s is nearly the same for C_6^2 and C_6^1 and with $\tilde{\eta}_1=0.4$ is well below the (planar) closed packed coverage, suggesting that the micelle–solvent interaction is moderate (for comparison see Ref. 14 for the adsorption of hard spheres on a sticky wall). θ_{12}^s is higher with $\tilde{\eta}_1=0.51$, though we then face the difficulty of interpretation mentioned previously. θ_{12}^s could be used to determine the magnitude of the micelle–solvent interaction but to our knowledge, it has not yet been measured by the experimental techniques which enable estimation of adsorption in related colloidal systems.[38]

V. CONCLUSION

The main conclusion we draw from this study is that for the micelles investigated, the change in effective adhesion (as evidenced from the experimental structure factor) is mostly due to the change in the overlap volume of the surface layers, independently of the actual magnitude of this adhesion and for any reasonable representation of the self adhesion of the solvent. If a simultaneous change of the micelle–solvent interaction occurs as for the smallest micelle, it should be rather weak. This interaction makes the micellar surface being not fully covered.

This study confirms the role of the overlap volume evidenced by Brunetti *et al.* But in contrast with their approach in which it is not obvious to understand how all the contributions to the potential of mean force ultimately sum up to give an attractive contribution almost proportional to the overlap volume, this volume appears in our approach in its natural place, that is in the direct intermicellar interaction. The possibility of interpreting then the variation in the *effective* interaction mostly from the change in *direct* intermicellar interaction indicates that other influential factors such as the steric effects, the solvent–solvent interaction and the micelle–solvent interaction are not significantly affected by modifications in surface composition of the kind investigated here. A slight decrease of the micelle–solvent interaction is required only when micelles of same surface composition have significantly different radii. As shown in this work, a

detailed analysis of the role of such factors can be made only from a multicomponent approach, which in principle also enables analysis of other data such as for one microemulsion in various solvent or at different temperatures. However this work illustrates the difficulties of going beyond the qualitative aspects and outlines the need of several improvements, both in the theoretical techniques used for computing the structure and in the model of the various components of the suspension.

APPENDIX A

For a binary mixture, Eqs. (3) form a set of three coupled equations (two formally quadratic for λ_{11} and λ_{22} and one formally linear for λ_{12}) which can be solved only numerically. We found it convenient to rearrange these equations as follows. From the original Eq. (3) and by defining $u_1=x\eta_1-\tau_{11}$, $u_2=x\eta_2-\tau_{22}$, $v_1=(\eta_1/6)(2x+3\eta_1x^2)$, $v_2=(\eta_2/6)(2x+3\eta_2x^2)$, $n=(\eta_1\eta_2)/6$; $x=1/(1-\eta_1-\eta_2)$, $\epsilon\equiv y=D_1/D_2$, $\tilde{\eta}=\eta_1+\epsilon\eta_2$, $\lambda=\eta_1\lambda_{11}+\epsilon\eta_2\lambda_{22}$, $X(\lambda_{12})=3x^2-2x\lambda_{12}+(\lambda_{12}^2/6)$, we have

$$\frac{\eta_1\lambda_{11}}{6}=u_1-\sqrt{u_1^2-v_1-\epsilon nX(\lambda_{12})}, \tag{A1}$$

$$\frac{\eta_2\lambda_{22}}{6}=u_2-\sqrt{u_2^2-v_2-\epsilon^{-1}nX(\lambda_{12})}, \tag{A2}$$

$$\lambda_{12}=[x(1+\epsilon)+3x^2\tilde{\eta}-x\tilde{\lambda}]\left(\frac{4\epsilon}{1+\epsilon}\,\tau_{12}+x\tilde{\eta}-\frac{\tilde{\lambda}}{6}\right)^{-1}. \tag{A3}$$

Equations (A1) and (A2) can then be inserted into Eq. (A3) yielding a unique equation for the unknown λ_{12}. By a simple algebra, this equation can be further transformed into another equation for the auxillary variable $L=\sqrt{6n\epsilon}[x-(\lambda_{12}/6)]$:

$$\sqrt{\rho_1^2-L^2}+\sqrt{\rho_2^2-L^2}=C-\frac{K}{L}, \tag{A4}$$

where $C=u_1+\epsilon u_2-w$, $K=(D/6)\sqrt{6n\epsilon}$, $\rho_1^2=u_1^2-v_1+3\epsilon nx^2$, $\rho_2^2=\epsilon^2(u_2^2-v_2)+3\epsilon nx^2$ with $w=[(4\epsilon)/(1+\epsilon)]\tau_{12}+x\tilde{\eta}$, $z=x(1+\epsilon)+3x^2\tilde{\eta}$, $D=z-6xw$.

Equation (A4) has a very simple geometrical interpretation: The solutions for L (i.e., for λ_{12}) are such that the hyperbola defined by $H(L)=C-K/L$ intercepts the sum of the two semicircles of radii ρ_1 and ρ_2. The numerical search of the intercepts is then greatly simplified and fastened by geometrical considerations. Depending on the value of the parameters τ_{11}, τ_{22}, τ_{12}, η_1, and η_2, the value of C and the sign of K fix the position of the hyperbola with respect to the sum of semicircles so that the search can be switched to the correct range. Only the positive solutions for λ_{11}, λ_{22}, and λ_{12} verifying $\det\mathbf{Q}(0)>0$ are finally retained. For all the parameter ranges discussed in the text, the solution was unique. For extreme (low) values however, a second set associated with high values of $S_{22}(0)$ (presumably corresponding to metastable states of the system) is sometimes found.

APPENDIX B

As mentioned in our previous work[22(b),24] τ_{22} obtained for the fit may also partly reflect the artificial adhesion which is necessary for forcing the PYA to reproduce the correct effective adhesion associated with the purely steric effect, since it otherwise underestimates it.[11] Comparing τ_{22}^f and τ_{22}^{eq} is thus correct only if τ_{22}^f reflects mostly the real adhesion. Both effects are difficult to separate, but a rough estimation can be made by adding to the true potential $U_{22}(r)$ a square well of depth ϵ^{PY} for $D_2\leqslant r\leqslant D_2+\delta^{PY}$ which would simulate the artificial adhesion necessary for correcting the PYA results for hard spheres. We may then compare the effective stickiness parameter τ_{22}^{eff} [via Eq. (6)] in the presence of this artificial well with the real one τ_{22}^{eq} in its absence. Assuming $\epsilon^{PY}\ll kT$ and linearizing $\exp(\beta\epsilon^{PY})$ we obtain

$$\frac{1}{\tau_{22}^{eff}}=\frac{1}{\tau_{22}^{eq}}(1+\beta\epsilon^{PY})+\frac{1}{\tau^{PY}},$$

where $1/\tau^{PY}=4\beta\epsilon^{PY}[(1+\delta^{PY})^3-1]$ is the inverse stickiness associated with the correction. We anticipate that the lower τ_{22}^f, the more it will reflect the real adhesion since the influence of this artificial well will then be negligible. Taking for example $\epsilon^{PY}=0.1$ kT and $\delta^{PY}=0.3D_2$ gives $\tau^{PY}=2.09$ [for hard spheres with $y=0.1$, a correction by $\tau_{22}=2$ was found[22(b)] to give a very large increase of $S_{22}(0)$] compared with $\tau_{22}=\infty$. Then $\tau_{22}^{eff}=0.15$ would correspond to $\tau_{22}^{eq}=0.18$ and $\tau_{22}^{eff}=0.5$ to $\tau_{22}^{eq}=0.72$. Incidentally, the overall effect of this correction is to bring the solid circles in Fig. 7 closer on average to the line of unit slope. Although the precise correction is unknown a correction similar to that estimated for hard spheres will thus not destroy the correlation observed here.

[1] S. Brunetti, D. Roux, A. M. Bellocq, G. Fourche, and P. Bothorel, J. Phys. Chem. **87**, 1028 (1983).
[2] B. Lemaire, P. Bothorel, and D. Roux, J. Phys. Chem. **87**, 1023 (1983).
[3] D. Roux, Thesis, Université de Bordeaux I, 1984.
[4] J. S. Van Duijneveldt, A. W. Heinen, and H. N. W. Lekkerkerker Europhys. Lett. **21**, 369 (1993).
[5] S. Sanyal, N. Easwar, S. Ramaswamy, and A. K. Sood, Europhys. Lett. **18**, 107 (1992).
[6] C. G. de Kruif, W. J. Briels, R. P. May, and A. Vrij, Langmuir **4**, 668 (1988).
[7] C. G. de Kruif, P. W. Rouw, W. J. Briels, M. H. G. Duits, A. Vrij, and R. P. May, Langmuir **5**, 422 (1989).
[8] C. Robertus, J. G. H. Joosten, and K. Levine, J. Chem. Phys. **93**, 7293 (1990).
[9] G. Cassin, J. P. Badiali, and M. P. Pileni, J. Phys. Chem. **99**, 12941 (1995).
[10] Y. Rosenfeld, Phys. Rev. Lett. **72**, 3831 (1994).
[11] T. Biben and J. P. Hansen, Phys. Rev. Lett. **66**, 2215 (1991).
[12] R. J. Baxter, J. Chem. Phys. **49**, 2770 (1968).
[13] J. W. Perram and E. R. Smith, Chem. Phys. Lett. **35**, 138 (1975).
[14] B. Barboy, Chem. Phys. **11**, 357 (1975); B. Barboy and R. Tenne, *ibid*. **38**, 369 (1978).
[15] G. Stell, J. Stat. Phys. **63**, 1203 (1991).
[16] E. R. Smith and J. W. Perram, J. Stat. Phys. **17**, 47 (1977).
[17] E. Dickinson, J. Chem. Soc. Faraday Trans. **88**, 3561 (1992).
[18] C. Robertus, W. H. Philipse, J. G. H. Joosten, and K. Levine, J. Chem. Phys. **90**, 4482 (1989).
[19] Y. C. Chiew and E. D. Glandt, J. Phys. A: Math. Gen. **22**, 3969 (1989); Y. C. Chiew, J. Colloid Interface Sci. **143**, 397 (1991).

[20] A. Jamnik, D. Bratko, and D. J. Henderson, J. Chem. Phys. **94**, 8210 (1991).
[21] M. H. G. M. Penders and A. Vrij, Physica A, **173**, 532 (1991); Progr. Colloid Polym. Sci **88**, 1 (1992).
[22] (a) Y. Heno and C. Regnaut, C R Acad. Sci. Paris **315**, 163 (1992); (b) C. Regnaut, S. Amokrane, and Y. Heno, J. Chem. Phys. **102**, 6230 (1995).
[23] E. Dickinson, J. Chem. Soc. Faraday Trans. **91**, 4413 (1995).
[24] (a) S. Amokrane, P. Bobola, and C. Regnaut, Prog. Colloid Polym. Sci **100**, 186 (1996); (b) Europhys. Conf. Abstr., edited by R. M. Pick, 3rd liquid matter conf. 20b, P7-22 (1996).
[25] C. Regnaut and J. C. Ravey, J. Chem. Phys. **91**, 1211 (1989).
[26] S. V. G. Menon, C. Manohar, and K. Srinivasa Rao, J. Chem. Phys. **95**, 9186 (1991).
[27] K. Shukla and R. Rajagopalan, Mol. Phys. **81**, 1093 (1994).
[28] J. Bergenholtz, P. Wu, N. J. Wagner, and B. D'Aguano, Mol. Phys. **87**, 331 (1996).
[29] W. R. Smith, D. Henderson, and Y. Tago, J. Chem. Phys. **67**, 5308 (1977); D. Henderson, O. H. Scalise, and W. R. Smith, *ibid*. **72**, 2431 (1980).
[30] D. M. Heyes and P. J. Aston, J. Chem. Phys. **97**, 5738 (1992).
[31] S. Bravo Yuste and A. Santos, J. Chem. Phys. **101**, 2355 (1994).
[32] Y. Zhou, C. K. Hall, and G. Stell, Mol. Phys. **86**, 1485 (1995).
[33] (a) R. C. Reid, J. M. Prausnitz, and B. E. Poling, *The Properties of Liquids and Gases* (McGraw-Hill, NY, 1987) p. 40; (b) J. H. Dymond, Fluid Phase Equil. **27**, 1 (1986).
[34] S. J. Smithline and A. D. Haymet, J. Chem. Phys. **83**, 4103 (1985); C. F. Tejero and M. Baus, Phys. Rev B **48**, 3793 (1993); D. W. Marr and P. Gast, J. Chem. Phys. **99**, 23024 (1993).
[35] R. Penfold, S. Abbas, and S. Nordholm, Fluid Phase Equil. **120**, 39 (1996); Europhys. Conf. Abstr., edited by R. M. Pick, 3rd liquid matter conf. 20b, P6-27 (1996).
[36] A. Luzar and D. Bratko, J. Chem. Phys. **92**, 642 (1990); D. Bratko, C. E. Woodward, and A. Luzar, J. Chem. Phys. **95**, 5318 (1991).
[37] N. F. Carnahan and K. E. Starling, J. Chem. Phys. **51**, 635 (1969).
[38] R. H. Ottewill, Progr. Colloid Polym. Sci. **88**, 49 (1992).